ULTRACOLD CHEMISTRY

Reactions between layer-resolved molecules mediated by dipolar spin exchange

William G. Tobias*, Kyle Matsuda, Jun-Ru Li, Calder Miller, Annette N. Carroll, Thomas Bilitewski, Ana Maria Rey, Jun Ye*

Microscopic control over polar molecules with tunable interactions enables the realization of distinct quantum phenomena. Using an electric field gradient, we demonstrated layer-resolved state preparation and imaging of ultracold potassium-rubidium molecules confined to two-dimensional planes in an optical lattice. The rotational coherence was maximized by rotating the electric field relative to the light polarization for state-insensitive trapping. Spatially separated molecules in adjacent layers interact through dipolar spin exchange of rotational angular momentum; by adjusting these interactions, we regulated the local chemical reaction rate. The resonance width of the exchange process vastly exceeded the dipolar interaction energy, an effect attributed to thermal energy. This work realized precise control of interacting molecules, enabling electric field microscopy on subwavelength scales and allowing access to unexplored physics in two-dimensional systems.

Ultracold polar molecules, which have complex internal structures and dipole moments tunable with external electric fields, represent a model system for studying many-body physics (*1*–*4*). In reduced dimensionality, the sign and magnitude of interactions between molecules depend on the orientation of the dipole moments with respect to the external confinement. Within two-dimensional (2D) layers, for example, the averaged interactions between molecules can be varied continuously from attractive to repulsive by rotating the dipoles into and out of the plane. Molecules in an isolated 2D layer are predicted to exhibit diverse quantum phenomena determined by the dipole angle and other parameters, including electric field and rotational state. These include complex ground state phases, such as superfluids and topological insulators (*5*–*12*), collective excitations in the hydrodynamic regime (*13*), and interaction-enhanced rotational coherence and dynamical generation of spin squeezing (*14*). Molecules prepared in multiple 2D layers may pair and form states with long-range order (*15*–*18*). Addressing individual lattice layers would allow initialization of varied configurations to realize these models—single layers, where molecules are isolated against out-of-plane interactions, and minimal systems with interlayer interactions, such as bilayers and trilayers (two and three adjacent layers, respectively).

Recent experimental progress with molecules in two dimensions has included reaching quantum degeneracy using direct evaporation (*19*) or pairing in a degenerate atomic gas (*20*), performing optical microscopy of individual lattice sites (*21*), and lengthening the coherence time of rotational superpositions (*22*, *23*). When translational motion is allowed within layers, as is the case for confinement in a 1D optical lattice, molecules approaching at short range undergo lossy chemical reactions (*24*–*28*). These losses can be mitigated by orienting the dipole moments perpendicular to the layer (*19*, *29*–*32*) or by engineering rotational state couplings (*33*–*37*) to generate a repulsive collisional barrier. A major missing capability is the ability to prepare molecules in different internal states and control multiple layers individually, which permits local tuning of dipolar interactions in reduced dimensionality.

In this work, we demonstrated layer-resolved imaging and rotational state preparation of ultracold potassium-rubidium (KRb) molecules by applying an electric field gradient to shift rotational transition frequencies between lattice layers. This method was inspired by previous works with atoms (*38*–*40*). Using the capability to address single layers, we characterized the dynamics of highly controlled few-layer systems interacting by exchanging rotational angular momenta (referred to as spin exchange), a process mediated by dipolar interactions (*41*). Within individual layers, molecules experience both long-range dipolar interactions and short-range chemical reactions, and separated layers only interact through dipolar spin exchange. In the case of multiple layers containing different rotational states, spin exchange led to mixing of rotational state populations, which strongly enhanced the chemical reaction rate (*42*). Local control of molecule layer occupation and internal state allowed us to probe these dynamics and would potentially enable the exploration of quantum phases in two dimensions.

Starting with degenerate ^{40}K and ^{87}Rb atoms in an optical dipole trap (ODT), we loaded a 1D optical lattice to form a stack of 2D layers with an interlayer spacing a = 540 nm (*19*). Using magnetoassociation and stimulated Raman adiabatic passage (STIRAP) at a bias electric field $|\mathbf{E}| = 1\,\mathrm{kV\,cm^{-1}}$, we associated the atoms into KRb (*43*, *44*). KRb was formed in the rotational ground state $|0\rangle$, where $|N\rangle$ denotes the state with electric field–dressed rotational quantum number N and zero angular momentum projection (m_N = 0) onto the quantization axis specified by $\mathbf{E}$ (*45*). The harmonic trapping frequencies for $|0\rangle$ in the combined trap were $(\omega_x, \omega_y, \omega_z) = 2\pi \times (42, 17 \times 10^3, 48)$ Hz. The molecules were pinned along **y**, parallel to gravity, but they were free to move radially (**x**-**z** plane; Fig. 1A). For the typical temperature T = 350 nK, $k_B T = 0.4\,\hbar\omega_y$, where k_B is the Boltzmann constant and $\hbar = h/2\pi$ is the reduced Planck constant, so the molecules

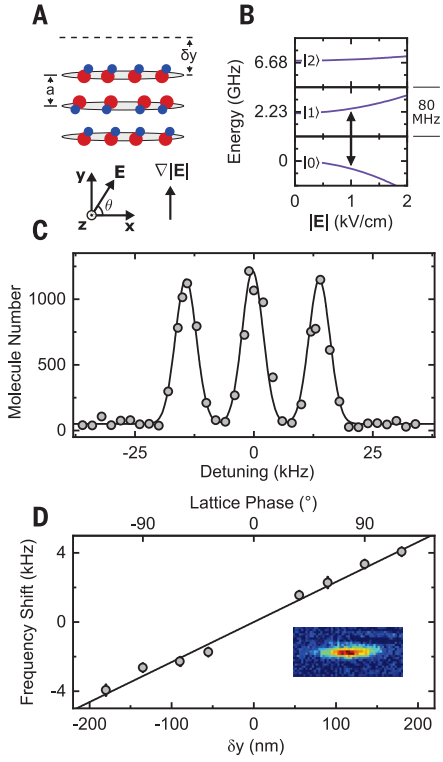

Fig. 1. Experimental configuration and individual layer addressing. (**A**) Molecules occupied 2D layers in the **x**-**z** plane, separated by layer spacing a. The bias electric field **E** was oriented at an angle θ in the **x**-**y** plane, with an electric field gradient $\nabla|\mathbf{E}|$ parallel to **y**. The lattice layers were displaced relative to the electrodes generating **E** by a distance δy. (**B**) KRb rotational structure. The arrow indicates the layer selection transition. (**C**) $|0\rangle \leftrightarrow |1\rangle$ frequency spectrum of a trilayer at $\partial_y|\mathbf{E}| = 6.4(2)\,\mathrm{kV\,cm^{-2}}$. Only three adjacent lattice layers were populated. (**D**) Center frequency shift of layer selection versus δy. Displacements smaller than 20 nm were measured. Error bars are 1 standard error from fits to the rotational transition line shape. (Inset) Absorption image of a single layer.

JILA, National Institute of Standards and Technology, and Department of Physics, University of Colorado, Boulder, CO 80309, USA.
*Corresponding author. Email: william.tobias@colorado.edu (W.G.T.); ye@jila.colorado.edu (J.Y.)

predominantly occupied the lowest lattice band. Because of the thermal extent of the atomic clouds along **y** before loading the optical lattice, the initial molecule distribution spanned ~12 lattice layers, with a peak of ~1500 molecules per layer. Compared with our previous work in two dimensions (*19*), where an auxiliary optical trap was used to compress KRb into few lattice layers to increase peak density, we deliberately prepared a broad distribution of molecules to minimize population differences among the central layers before layer addressing.

We generated highly configurable electric fields in the **x**-**y** plane using a set of six in-vacuum electrodes (*19*, *33*, *46*). To orient the induced dipole moments of the molecules, we rotated **E** by a variable angle θ, where θ = 0° corresponds to $\mathbf{E} \| \mathbf{x}$ (Fig. 1A). An electric field gradient $\nabla|\mathbf{E}|$ could be applied along **y**, parallel to the direction of tight confinement in the optical lattice. Because the KRb rotational energy levels are sensitive to $|\mathbf{E}|$, addressing single layers required stabilizing the molecule position relative to the local electric field distribution; such stabilization was accomplished by interferometrically measuring the positions of the lattice layers and electrodes and minimizing relative displacements (*45*). By adding a fixed phase offset to one of the beams generating the lattice, the layers were displaced from the electrodes along **y** by a distance δy. Using microwave pulses, the molecules could be transferred between states $|0\rangle$, $|1\rangle$, and $|2\rangle$ (Fig. 1B). Each rotational state $|N\rangle$ has an induced dipole moment d_N parallel to **E**, the magnitude of which depends on $|\mathbf{E}|$, leading to a state-dependent energy shift of $-d_N|\mathbf{E}|$. At $|\mathbf{E}| = 1$ kV cm^{-1}, where all subsequent measurements were performed, the sensitivity of the $|0\rangle \leftrightarrow |1\rangle$ transition to $|\mathbf{E}|$ is 40 kHz (V cm^{-1})$^{-1}$.

The electric field dependence of rotational state energies enabled microwave addressing of individual lattice layers. In terms of the layer spacing a and the dipole moments d_0 and d_1, a field gradient $\partial_y|\mathbf{E}|$ shifts the $|0\rangle \leftrightarrow |1\rangle$ transition on adjacent layers by the frequency

$$\Delta = \partial_y|\mathbf{E}| \cdot a \cdot \frac{d_0 - d_1}{h} \quad (1)$$

With a microwave pulse of sufficiently narrow spectral width, all molecules in a single layer could be addressed without a measurable effect on other layers. In addition to layer-selective addressing of the $|0\rangle \leftrightarrow |1\rangle$ transition, we had the capability to apply global microwave pulses (addressing all molecules, irrespective of $\partial_y|\mathbf{E}|$) on the $|0\rangle \leftrightarrow |1\rangle$ and $|1\rangle \leftrightarrow |2\rangle$ transitions, as well as to globally remove $|0\rangle$ and $|1\rangle$ molecules with optical pulses of STIRAP light. From an initial condition of many occupied $|0\rangle$ layers, we used sequences of these microwave and optical pulses to prepare arbitrary layer configurations containing states $|0\rangle$, $|1\rangle$, and $|2\rangle$, including isolated 2D layers (*45*).

To demonstrate layer selection, we prepared three adjacent layers in $|1\rangle$ and scanned the frequency of an additional layer-selective $|0\rangle \leftrightarrow |1\rangle$ pulse in an applied gradient $\partial_y|\mathbf{E}| = 6.4(2)$ kV cm^{-2}. By monitoring the population transferred to $|0\rangle$ as a function of frequency, we probed the initial $|1\rangle$ distribution (Fig. 1C). We measured ~1200 molecules in each occupied layer, with adjacent layers detuned by 14 kHz. No molecules were measured in layers outside the trilayer or between occupied layers, which confirmed that the pulses were selectively addressing individual layers.

By varying the layer displacement δy and tracking the layer selection transition frequency, $|\mathbf{E}(y)|$ could be extracted with high spatial resolution, far below the interlayer spacing of 540 nm or the imaging diffraction limit. To characterize this technique, we probed an applied gradient of $\partial_y|\mathbf{E}| = 6.4(2)$ kV cm^{-2}. At each of eight different values of δy, spanning 360 nm (corresponding to a lattice phase shift of 240°), we measured the central frequency for layer selection (Fig. 1D). Fitting the frequency shift as a function of δy, we extracted $\partial_y|\mathbf{E}| = 5.8(3)$ kV cm^{-2}, with a maximum offset between δy and the line of best fit of only 20 nm. These measurements demonstrated subwavelength detection of molecule distributions using electric field gradients and high-precision electric field microscopy on nanometer spatial scales.

Using layer-selective addressing, we next optimized the rotational coherence in a single layer. Long-lived coherence is essential for realizing strong dipolar interactions (*9*, *14*). However, inhomogeneous broadening from external electric fields and optical trapping potentials tends to limit coherence. Because the molecules in two dimensions occupied a large spatial extent in the radial direction, electric field gradients transverse to **y** contribute a position-dependent frequency shift between rotational states (Fig. 1A). Spatial variation in the optical trap intensity contributes an additional frequency shift because of the differential ac polarizability between rotational states. The magnitude of the shift depends on $|\mathbf{E}|$ as well as the angle between the quantization axis (aligned with **E**) and the optical lattice polarization $\boldsymbol{\varepsilon}$ (*47*). In our apparatus, because the optical lattice polarization $\boldsymbol{\varepsilon}$ was fixed parallel to **x**, this angle coincided with the rotation angle θ of **E** (Fig. 1A). State-insensitive trapping can be achieved at the so-called magic

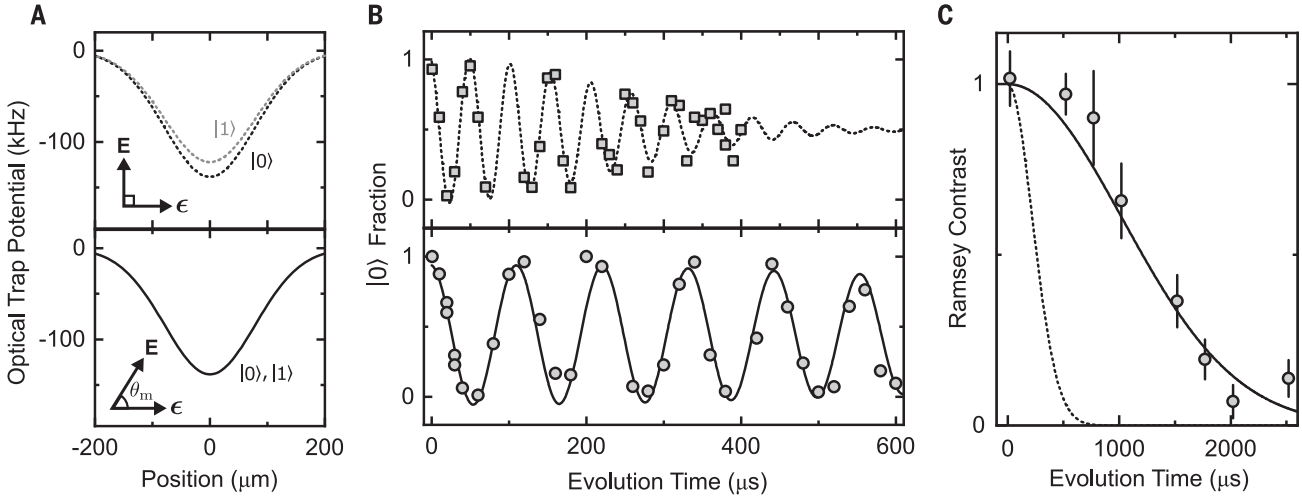

Fig. 2. Increasing rotational coherence time by rotating E. (**A**) Calculated optical trap potentials for states $|0\rangle$ and $|1\rangle$ in the ODT and optical lattice. The differential polarizability between rotational states depends on the angle θ between **E** and the optical lattice polarization $\boldsymbol{\varepsilon}$ and vanishes at $\theta_m \approx 54°$. (**B**) Ramsey oscillations of a single layer of molecules at θ = 90° (top, dashed line) and θ = θ_m (bottom, solid line). (**C**) Contrast of Ramsey fringes at long evolution times. The coherence time at θ = θ_m (points, solid line) was increased by a factor of 5 compared with θ = 90° (dashed line). Error bars are 1 standard error, estimated by simulations (*45*).

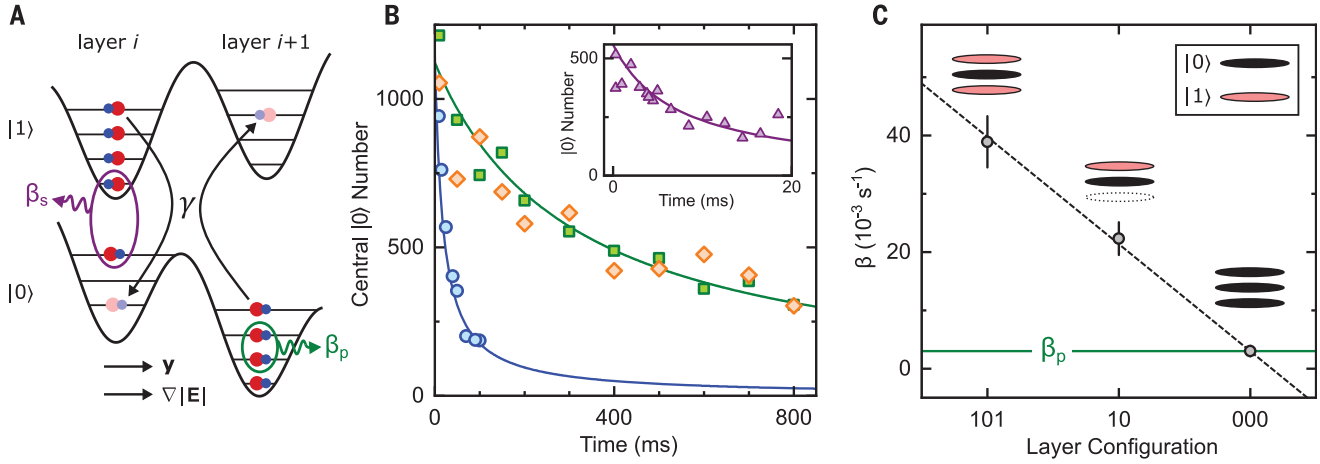

Fig. 3. Interaction and loss dynamics for molecules in two dimensions. (**A**) In a single layer, molecules in the same and in different rotational states undergo two-body loss with rate coefficients β_p and β_s, respectively. Molecules in different rotational states in adjacent layers may also exchange rotational states with rate γ, potentially changing harmonic oscillator modes during the exchange. (**B**) Central layer $|0\rangle$ molecule number versus time for 000 (β_p, green squares), 101 (blue circles), and 202 (orange diamonds) trilayers. The solid lines are fits to the two-body loss rate equation. (Inset) Loss for an equal mixture of molecules in states $|0\rangle$ and $|1\rangle$ (β_s). (**C**) Density dependence of spin exchange. β fit to the loss of $|0\rangle$ from layer configurations 000, 10, and 101 scaled linearly with the number of adjacent layers containing $|1\rangle$. The solid green line indicates β_p. Error bars are 1 standard error from fits to the two-body loss rate equation.

angle of ~54°, where the differential ac polarizability between all rotational states with m_N = 0 vanishes (Fig. 2A).

We measured the Ramsey coherence of a single 2D layer with $\partial_y|\mathbf{E}| = 0$ at both $\theta = 90°$ and $\theta = \theta_m$, where we define θ_m as the electric field angle at which we measured the minimum differential polarizability (*45*). For both angles, the ODT polarization was set to the magic angle with respect to **E**. Using a single layer removed possible systematics, such as dipolar interactions between layers, stray electric field gradients along **y**, and layer-to-layer optical trap intensity variation. To measure the coherence decay, we prepared a single layer of molecules, used a $\pi/2$ pulse to initialize all molecules on the layer in an equal superposition of $|0\rangle$ and $|1\rangle$, held for a variable evolution time, applied a second $\pi/2$ pulse, and simultaneously measured the population in both states. As a function of evolution time t, we fit the contrast envelope to the Gaussian function e^{-t^2/τ^2}, where τ is the coherence time. For $\theta = 90°$, we measured τ = 310(30) μs (Fig. 2B, top). This result was consistent with simulations where the differential ac polarizability was the only mechanism causing decoherence (*45*).

At $\theta = \theta_m$, little contrast decay was observed over the course of 600 μs (Fig. 2B, bottom). At longer evolution times, the Ramsey oscillation phase was scrambled by slight changes in $|\mathbf{E}|$ between experimental runs. We therefore computed the contrast on the basis of the observed variance of the rotational state populations (*45*). We measured τ = 1450(80) μs (Fig. 2C)—a factor of 5 improvement over $\theta = 90°$ and exceeding the longest bulk coherence time previously observed for KRb (*22*). Factors that may have limited the maximum achieved coherence included any remaining differential ac polarizability, residual electric field gradients, and intralayer dipolar interactions. With millisecond-scale coherence times and realistic experimental parameters, KRb is predicted to dynamically generate spin-squeezed states in two dimensions (*14*).

The capability to prepare arbitrary layer configurations enables the realization of new interacting systems. In this work, we studied a system where the rate of chemical reactions on a single 2D layer could be controlled by the presence of adjacent layers (*42*). The dynamics of molecules on multiple layers depend on a number of processes (Fig. 3A). In a single layer, molecules undergo two-body chemical reactions according to the rate equation $dN/dt = -\beta N^2$, where N is the molecule number and β is the two-body rate coefficient. KRb is fermionic, so ultracold molecules in the same internal state undergo reactions in the p-wave channel, with rate coefficient β_p. Molecules in different rotational states are distinguishable and therefore react in the s-wave channel, with rate coefficient β_s, which is typically orders of magnitude higher than β_p because of the absence of a centrifugal barrier (*24*, *48*). Molecules in separate layers in different rotational states may also exchange rotational angular momenta through long-range dipolar interactions (*41*), changing harmonic oscillator modes in the process (represented by γ in Fig. 3A). Spin exchange can only occur between states of opposite parity, meaning that $|0\rangle \leftrightarrow |1\rangle$ exchange is allowed and $|0\rangle \leftrightarrow |2\rangle$ exchange is forbidden at $|\mathbf{E}| = 0$. Applying an electric field induces rotational state mixing, but this effect only slightly weakens the above selection rules at $|\mathbf{E}| = 1\,\mathrm{kV\,cm^{-1}}$ (*45*).

Spin exchange facilitates the mixing of rotational state populations between initially spin-polarized layers, causing molecules undergoing exchange to be rapidly lost with rate coefficient β_s (*42*). To distinguish exchange from chemical reactions, we first measured the rate coefficients β_p and β_s at the temperature T = 334(30) nK, with $\nabla|\mathbf{E}| = 0$. Throughout the following, we describe bilayer and trilayer configurations according to the rotational states present in layers containing molecules. For example, 202 refers to a central layer containing only molecules of state $|0\rangle$ with adjacent $|2\rangle$ layers above and below and all other layers unoccupied. To extract β_p, which in general depends on rotational state because of variation in the intermolecular potentials (*49*), we prepared spin-polarized 000 (Fig. 3B, green squares), 111, and 222 trilayers and fit the number decay to the two-body loss rate equation. For $|0\rangle$ and $|1\rangle$, $\beta_p = 2.99(17) \times 10^{-3}\ \mathrm{s^{-1}}$. For $|2\rangle$, the loss rate was reduced to $\beta_p = 1.78(24) \times 10^{-3}\ \mathrm{s^{-1}}$. To extract β_s, we prepared a 111 trilayer and applied a $\pi/2$ pulse to form an equal superposition of $|0\rangle$ and $|1\rangle$, which decohered completely within several milliseconds (Fig. 3B, inset). We measured $\beta_s = 2.0(3) \times 10^{-1}\ \mathrm{s^{-1}}$, nearly two orders of magnitude larger than β_p, as has been previously observed (*24*).

The interplay of exchange and loss was evident in layer configurations where multiple rotational states were present. In a 202 trilayer, where selection rules prohibit spin exchange, the loss rate of $|0\rangle$ molecules from the central layer matched β_p (Fig. 3B, orange

diamonds). By contrast, for a 101 trilayer, the effective two-body loss rate increased by more than a factor of 10 (Fig. 3B, blue circles). The spin exchange rate depended on the density of molecules in adjacent layers, which is analogous to the dependence of the chemical reaction rate on the local molecule density. We demonstrated this effect by preparing 000, 10, and 101 layer configurations and fitting the decay of $|0\rangle$ molecules in the central layer to the two-body loss rate equation. The fit β scaled linearly with the number of adjacent $|1\rangle$ layers (Fig. 3C). These results showed the dependence of spin exchange on density and rotational state and demonstrated tuning of the chemical reaction rate using experimental control of the layer configuration.

To extract the spin exchange rate quantitatively, we described N_i^σ, the molecule number in layer i and in rotational state $|\sigma\rangle$, by a set of coupled differential equations including the aforementioned loss and exchange processes

$$\frac{dN_i^\sigma}{dt} = -\beta_p N_i^\sigma N_i^\sigma - \beta_s N_i^\sigma N_i^{\sigma'} + \gamma \sum_{k=i\pm1} \left(N_i^{\sigma'} N_k^\sigma - N_i^\sigma N_k^{\sigma'}\right) \quad (2)$$

where $\sigma \neq \sigma'$ are the two rotational states participating in the dynamics. The first two terms represent intralayer two-body loss, with rates β_p and β_s for spin-polarized and spin-mixed molecules, respectively. The third term represents spin exchange, which depends on the molecule populations in different rotational states in adjacent layers, occurring with rate constant γ (Fig. 3A). γ is an effective parameter describing the spin exchange, averaged over all molecules and over the full duration of the measurement.

Because spin exchange is a resonant process, adding an energy offset between adjacent layers suppresses its rate. To probe the energy spectrum of exchange, we added a variable gradient $\partial_y|\mathbf{E}|$ (Fig. 3A). The total change in electric potential energy when molecules in adjacent layers exchange rotational states is $h\Delta$ (Eq. 1), which is equivalent to the shift in microwave transition energy between adjacent layers (Fig. 1C). For states $|0\rangle$ and $|1\rangle$, Δ = 14 kHz at $\partial_y|\mathbf{E}| = 6.4\,\mathrm{kV\,cm^{-1}}$, the gradient used for layer selection.

We measured the spin exchange rate γ as a function of Δ in 101 and 202 trilayer configurations (Fig. 4A), with $\theta = 90°$ and at T = 334(30) nK. For 202, the measured γ was consistent with zero spin exchange and did not depend on Δ. For 101, however, the peak exchange rate was $\gamma = 7.0(6) \times 10^{-3}\ \mathrm{s^{-1}}$, more than two times β_p. Notably, γ remained nonzero for large Δ, with a Lorentzian fit to $\gamma(\Delta)$ having a full width at half maximum (FWHM) of 6.4(6) kHz. This energy scale vastly exceeded the dipolar interaction energy between two molecules: At a separation of 540 nm, the rate of spin exchange between molecules in $|0\rangle$ and $|1\rangle$ is only 100 Hz (*41*).

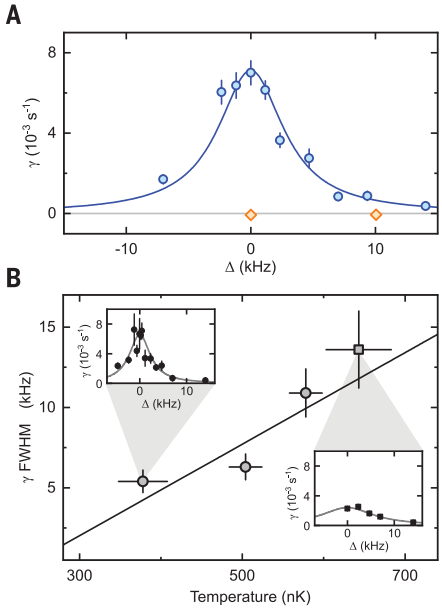

Fig. 4. Dependence of spin exchange on interlayer detuning Δ, rotational state, and temperature. (**A**) Spin exchange rate versus Δ, with $\theta = 90°$ and T = 334(30) nK, for 101 (blue circles) and 202 (orange diamonds) trilayers. The solid line is a Lorentzian fit to extract the FWHM. The point displayed at Δ = 0 kHz is the weighted average of measurements at Δ = 0 and ±0.12 kHz. (**B**) Temperature dependence of spin exchange linewidth, with $\theta = \theta_m$. The solid line is a linear fit for the temperature range shown. (Insets) γ versus Δ at T = 378(30) nK (circles, upper inset) and T = 643(40) nK (squares, lower inset). Error bars are 1 standard error from fits to Eq. 2.

Thermal energy contributed to the broad linewidth. To compensate Δ and conserve energy during spin exchange, molecules must change harmonic modes (Fig. 3A), the initial occupation of which is determined by the temperature. Qualitatively, this mechanism gives insight into the scaling of γ with T and Δ. At low temperatures, no spin exchange can occur when Δ greatly exceeds the thermal energy. For small Δ, however, the spin exchange rate is enhanced because of the high average occupation and strong dipolar coupling of low-lying harmonic modes. At high temperatures, the situation is reversed: High-lying modes are occupied, allowing exchange even at large Δ, but the peak exchange rate on resonance is suppressed. These effects suggest that increasing the temperature should broaden the spin exchange linewidth.

To quantify the temperature dependence, we repeated the measurement of $\gamma(\Delta)$ with a 101 trilayer at four temperatures between 370 and 650 nK (Fig. 4B). We set $\theta = \theta_m$ to eliminate possible broadening because of varying trap potentials between rotational states (Fig. 2A). At this angle, the strength of dipolar interactions between harmonic modes was slightly altered because the dipole moments were rotated relative to the plane of motion. At the lowest temperature, we measured a FWHM of 5.4(7) kHz, only slightly narrower than at $\theta = 90°$. At the highest temperature, by contrast, the peak γ was reduced and the FWHM more than doubled to 13.6(2.4) kHz. To provide physical insight into the temperature dependence, we developed a simple two-particle model of molecules in adjacent layers interacting through dipolar spin exchange (*45*). Weighting by the thermal mode occupation, we found qualitative agreement with the observed trend. In addition to thermal energy, effects that may contribute to broadening include many-body interactions, where multiple molecules participate jointly in the spin exchange process, and intralayer dipole-dipole interactions. Both of these mechanisms should only weakly affect the temperature scaling because of the relatively low molecule density and small dipole moments at $|\mathbf{E}| = 1\,\mathrm{kV\,cm^{-1}}$.

We have demonstrated experimental control over spin exchange and chemical reactions in 2D systems of ultracold molecules, enabled by subwavelength addressing of individual lattice layers. These results provide a general method for layer-resolved state preparation and imaging of polar molecules, facilitating the study of many-body phases and nonequilibrium dynamics in long-range interacting systems with reduced dimensionality.

REFERENCES AND NOTES

1. A. Micheli, G. K. Brennen, P. Zoller, *Nat. Phys.* **2**, 341–347 (2006).
2. K. Góral, L. Santos, M. Lewenstein, *Phys. Rev. Lett.* **88**, 170406 (2002).
3. M. A. Baranov, M. Dalmonte, G. Pupillo, P. Zoller, *Chem. Rev.* **112**, 5012–5061 (2012).
4. J. L. Bohn, A. M. Rey, J. Ye, *Science* **357**, 1002–1010 (2017).
5. N. Y. Yao *et al.*, *Phys. Rev. Lett.* **110**, 185302 (2013).
6. A. V. Gorshkov *et al.*, *Phys. Rev. A* **84**, 033619 (2011).
7. S. R. Manmana, E. M. Stoudenmire, K. R. A. Hazzard, A. M. Rey, A. V. Gorshkov, *Phys. Rev. B* **87**, 081106 (2013).
8. N. Y. Yao, M. P. Zaletel, D. M. Stamper-Kurn, A. Vishwanath, *Nat. Phys.* **14**, 405–410 (2018).
9. D. Peter, S. Müller, S. Wessel, H. P. Büchler, *Phys. Rev. Lett.* **109**, 025303 (2012).
10. S. V. Syzranov, M. L. Wall, V. Gurarie, A. M. Rey, *Nat. Commun.* **5**, 5391 (2014).
11. N. R. Cooper, G. V. Shlyapnikov, *Phys. Rev. Lett.* **103**, 155302 (2009).
12. J. Levinsen, N. R. Cooper, G. V. Shlyapnikov, *Phys. Rev. A* **84**, 013603 (2011).
13. M. Babadi, E. Demler, *Phys. Rev. A* **86**, 063638 (2012).
14. T. Bilitewski *et al.*, *Phys. Rev. Lett.* **126**, 113401 (2021).
15. D.-W. Wang, M. D. Lukin, E. Demler, *Phys. Rev. Lett.* **97**, 180413 (2006).
16. A. C. Potter, E. Berg, D.-W. Wang, B. I. Halperin, E. Demler, *Phys. Rev. Lett.* **105**, 220406 (2010).
17. A. Pikovski, M. Klawunn, G. V. Shlyapnikov, L. Santos, *Phys. Rev. Lett.* **105**, 215302 (2010).
18. N. T. Zinner, B. Wunsch, D. Pekker, D.-W. Wang, *Phys. Rev. A* **85**, 013603 (2012).
19. G. Valtolina *et al.*, *Nature* **588**, 239–243 (2020).
20. Z. Zhang, L. Chen, K.-X. Yao, C. Chin, *Nature* **592**, 708–711 (2021).
21. J. S. Rosenberg, L. Christakis, E. Guardado-Sanchez, Z. Z. Yan, W. S. Bakr, Observation of the Hanbury Brown and Twiss effect

with ultracold molecules. arXiv:2111.09426 [cond-mat.quant-gas] (2021).
22. B. Neyenhuis *et al*., *Phys. Rev. Lett.* **109**, 230403 (2012).
23. F. Seeßelberg *et al*., *Phys. Rev. Lett.* **121**, 253401 (2018).
24. S. Ospelkaus *et al*., *Science* **327**, 853–857 (2010).
25. M.-G. Hu *et al*., *Science* **366**, 1111–1115 (2019).
26. R. Bause *et al*., *Phys. Rev. Res.* **3**, 033013 (2021).
27. P. Gersema *et al*., *Phys. Rev. Lett.* **127**, 163401 (2021).
28. P. D. Gregory, J. A. Blackmore, S. L. Bromley, S. L. Cornish, *Phys. Rev. Lett.* **124**, 163402 (2020).
29. G. Quéméner, J. L. Bohn, *Phys. Rev. A* **81**, 060701 (2010).
30. K.-K. Ni *et al*., *Nature* **464**, 1324–1328 (2010).
31. M. H. G. de Miranda *et al*., *Nat. Phys.* **7**, 502–507 (2011).
32. A. Frisch *et al*., *Phys. Rev. Lett.* **115**, 203201 (2015).
33. K. Matsuda *et al*., *Science* **370**, 1324–1327 (2020).
34. J.-R. Li *et al*., *Nat. Phys.* **17**, 1144–1148 (2021).
35. L. Anderegg *et al*., *Science* **373**, 779–782 (2021).
36. G. Wang, G. Quéméner, *New J. Phys.* **17**, 035015 (2015).
37. T. Karman, J. M. Hutson, *Phys. Rev. Lett.* **121**, 163401 (2018).
38. M. Karski *et al*., *New J. Phys.* **12**, 065027 (2010).
39. J. F. Sherson *et al*., *Nature* **467**, 68–72 (2010).
40. G. J. A. Edge *et al*., *Phys. Rev. A* **92**, 063406 (2015).
41. B. Yan *et al*., *Nature* **501**, 521–525 (2013).
42. A. Pikovski, M. Klawunn, A. Recati, L. Santos, *Phys. Rev. A* **84**, 061605 (2011).
43. K.-K. Ni *et al*., *Science* **322**, 231–235 (2008).
44. L. De Marco *et al*., *Science* **363**, 853–856 (2019).
45. See the supplementary materials.
46. J. Covey, thesis, University of Colorado Boulder (2017).
47. S. Kotochigova, D. DeMille, *Phys. Rev. A* **82**, 063421 (2010).
48. Z. Idziaszek, P. S. Julienne, *Phys. Rev. Lett.* **104**, 113202 (2010).
49. S. Kotochigova, *New J. Phys.* **12**, 073041 (2010).
50. W. G. Tobias *et al*., Data for "Reactions between layer-resolved molecules mediated by dipolar spin exchange", version 1, Zenodo (2022); https://doi.org/10.5281/zenodo.6081435.

ACKNOWLEDGMENTS

We thank S. R. Cohen, L. De Marco, and G. Valtolina for experimental contributions and Y. Liu and C. Sanner for helpful discussions. **Funding:** This study received support from the Army Research Office, Multidisciplinary University Research Initiative; the Air Force Office of Scientific Research, Multidisciplinary University Research Initiative; the Defense Advanced Research Projects Agency, Driven and Nonequilibrium Quantum Systems; the National Science Foundation, Quantum Leap Challenge Institutes, Office of Multidisciplinary Activities (grant 2016244); the National Science Foundation (grant Phys-1734006); and the National Institute of Standards and Technology. **Author contributions:** Experimental work and data analysis: W.G.T., K.M., J.-R.L., C.M., A.N.C., and J.Y. Two-particle exchange model: T.B. and A.M.R. Interpreting results and writing the manuscript: W.G.T., K.M., J.-R.L., C.M., A.N.C., T.B., A.M.R., and J.Y. **Competing interests:** The authors declare no competing interests. **Data and materials availability:** All data needed to evaluate the conclusions in this paper are present in the paper or the supplementary materials and are available through Zenodo (*50*).

SUPPLEMENTARY MATERIALS

science.org/doi/10.1126/science.abn8525
Supplementary Text
Figs. S1 to S4

24 December 2021; accepted 15 February 2022
10.1126/science.abn8525

Science

Reactions between layer-resolved molecules mediated by dipolar spin exchange

William G. TobiasKyle MatsudaJun-Ru LiCalder MillerAnnette N. CarrollThomas BilitewskiAna Maria ReyJun Ye

Science, 375 (6586), • DOI: 10.1126/science.abn8525

Layers of ultracold chemistry

Ultracold polar molecules trapped in two-dimensional layers are predicted to exhibit complex quantum phenomena not available with other platforms because of long-range anisotropic and tunable dipolar interactions. Using precision electric field control, Tobias *et al*. demonstrated layer-resolved creation and imaging of ultracold potassium–rubidium molecules confined to two-dimensional planes in an optical lattice. They also studied spin exchange and chemical reactions, which are shown to be highly dependent on the molecule temperature and interlayer detunings introduced by an electric field gradient. This work demonstrates high control of ultracold molecules in an optical lattice and is a promising step toward exploring emerging phenomena in quantum gas systems with reduced dimensionality. —YS